Wandering of wing-tip vortices

A.L. Heyes, R.F. Jones and D.A.R. Smith

Department of Mechanical Engineering,
Imperial College London,
Exhibition Road, London, SW7 2AZ

Abstract

Vortex wakes are an example of flows which exhibit unsteadiness from sources other than turbulence. The phenomenon of vortex wandering is where the vortex core moves in an apparently random fashion relative to the fixed observer. This prevents reliable conclusions from being drawn from temporally averaged measurements which, for example, reduces their value for CFD validation unless its effects are dealt with. Previous studies have demonstrated possible strategies to extract reliable data from that affected by wandering, but the methods used are not necessarily universal or convenient. In this study we demonstrate a relatively simple method for recovering the vortex structure from flow-field data taken using PIV and compare with a statistically based method for carrying out the same. Data is presented showing that wandering amplitude increases linearly with stream-wise distance and also increases with background turbulence intensity, but decreases with vortex strength. Reliable data, corrected for the effects of wandering, shows that the vortex studied here grows at a more rapid rate than a Lamb-Oseen vortex undergoing viscous diffusion.

Nomenclature

b	half-span (mm).
c	chord (mm).
e	correlation coefficient between y and z rms wandering amplitudes.
k	cross stream fluctuation energy $0.5\left(\overline{v^2}+\overline{w^2}\right)$
r	radius (mm).
r_c	vortex core radius (mm).
t	time (s).
%Tu	Turbulence intensity (%).
U	mean velocity component in stream-wise, x direction (m/s).
U_{inf}	free stream velocity (m/s).
$\overline{v^2}$	Reynolds normal stress component in horizontal, y direction (m^2/s^2).
$\overline{vw}$	Reynolds shear stress component (m^2/s^2).
V	mean velocity component in horizontal, y direction (m/s).
V_θ	tangential velocity component (m/s).
$V_{\theta max}$	peak tangential velocity component at r_c (m/s).
$\overline{w^2}$	Reynolds normal stress component in vertical, z direction (m^2/s^2).
W	mean velocity component in vertical, z direction (m/s).

x	steam-wise co-ordinate direction (mm).
y	horizontal co-ordinate direction (mm).
z	vertical (span-wise) co-ordinate direction (mm).
α	angle of attack (degrees).
Δ	vector grid spacing (mm).
Γ	circulation (m^2/s).
Γ_{2rc}	circulation at $2r_c$ (m^2/s).
σ	rms wandering amplitude magnitude $\left(\sigma_y^2 + \sigma_z^2\right)^{0.5}$ (mm).
σ_y	rms wandering amplitude component in y direction (mm).
σ_z	rms wandering amplitude component in z direction (mm).
ν	kinematic viscosity (m^2/s).

1.0 Introduction

The hazard associated with aircraft vortex wakes is well-known and the ability to control their behaviour will bring benefits in terms of increased safety and air traffic capacity. Many previous studies present laboratory scale measurements of wakes of varying complexity from simple rectangular plan-form airfoils to detailed aircraft models, for example, Clifone (1976), deBruin et al (1996), Devenport et al (1996), Jacquin et al (2001) and Heunecke (2002) and an important feature of these flows is so-called "vortex wandering", that is the unsteady motion of the vortex core in the surrounding flow. Wandering has important consequences for the accuracy of measurements, since the use of uncorrected data to extract mean and fluctuating component gives a "smeared-out" version of the true flow field and can lead to false conclusions about derived quantities such as peak velocities and vortex core size. Furthermore, as demonstrated by Devenport et al (1996) wandering contributes to apparently high levels of Reynolds stresses in the vortex core which, in their case, was actually laminar. Therefore the ability to distinguish wandering in experimental data, to quantify its amplitude and to extract data with its effects removed is of utmost importance for the reliability of the data and for its value in validating CFD studies.

Following from Baker et al (1974), Devenport et al (1996) developed a theory to correct mean velocity fields for the effects of wandering, to estimate its amplitudes and its contribution to the Reynolds stresses. This process involves forming a "corrected" mean velocity field from the measured version, using guessed levels of wandering amplitude. This corrected field is then artificially subjected to wandering, described by a bi-variate Gaussian probability density function for vortex position, and the resulting Reynolds stresses at the vortex centre are compared with the actual measured values. The wandering amplitudes are then adjusted iteratively until the calculated and measured values converge. The authors made measurements of the development of a single tip-vortex from a rectangular plan-form NACA 0012 section wing of aspect ratio 4.3 at a chord Reynolds number of 5.3×10^5 using a special miniature 4-wire hot-wire probe. Using their wandering correction theory they found that the amplitude of wandering varied linearly between 0.1 and 0.4 vortex core radii at stream-wise distances of 5 to 36 chord-lengths and at its highest level, wandering was responsible for a 12% and 15%

error in the measured core radii and peak tangential velocity respectively. They concluded that the vortex core in their experiments was laminar and that velocity fluctuations here were entirely due to wandering and were at frequencies below $f=U_{inf}/c$.

Jacquin et al (2001) proposed four possible causes for wandering; perturbation of the vortex core by wind-tunnel unsteadiness, perturbation of the core by turbulence in the surrounding shear layer (as it rolls up around the core), co-operative instabilities (for example the Crow instability) or propagation of unsteadiness from the model. Intuitively buffeting of the core by unsteadiness in the wind tunnel free-stream is a likely cause and is often cited as such without further justification. However Jaquin et al (2001) carried out an original test which showed that wandering was apparently insensitive to free stream unsteadiness. Using a generic model of an Airbus A300 they placed a splitter plate which divided the tunnel into two sections, for a length of 8 spans, starting 1 span ahead of the model, the purpose of which was to generate a thick boundary layer in order to perturb the vortex. Whilst the mean position of the vortex was slightly altered no change in the velocity autospectra measured at the core centre was found with the presence of the plate. The velocity spectra did exhibit peaks, which lay close to the to the Crow frequency for the model used, however an accelerometer placed on the model showed that there were structural modes at these frequencies so the contribution could not be separated.

Rokhsaz (2000) carried out an investigation of wandering of a tip-vortex from a rectangular plan-form flat plate airfoil in a water tunnel and showed that wandering increased with angle of attack and therefore vortex strength, the opposite to the finding of Devenport et al. who show a 15% reduction in wandering amplitude with an increase in vortex strength of 85%. It may be the case, that flow separation occurring at the higher angles of attack used in Rokhsaz's experiment contributes to the rise in wandering. Gursul (2000) records a sharp rise in wandering above a certain threshold Reynolds number and attributes this to the onset of Kelvin-Helmholtz instability in the shear layer rolling around the vortex core.

In this paper a method for correcting velocity data for the effects of wandering is proposed and tested and the effects of vortex strength and free-stream turbulence on wandering are investigated. The development of the vortex from one data set is examined with the effects of wandering removed.

2.0 Flow configuration and instrumentation

The measurements presented herein were made in an open return wind-tunnel of 0.45 x 0.3m cross section and 2m in length. Wing models were mounted vertically upwards from the wind tunnel floor. Two models with chords of c=70mm and c=150mm and NACA 0012 section were used in this study, both with half span b=150mm. The free stream velocity was set to 21.6 m/s giving chord based Reynolds numbers of $Re_c=1 \times 10^5$ and 2.2×10^5. The main instrumentation comprised a LaVision Flowmaster PIV system with a New Wave Solo (120mJ) Nd:YAG laser, and a 12 bit, cooled CCD camera with 1360 x 1024 pixels fitted with a Tokina 70-210mm zoom lens and macro rings. The laser

was equipped with optics producing a light sheet which was focussed to approximately 2.0mm thick throughout the measurement region. The time between the laser pulses was set to be 15μs, giving acceptable particle displacements in the vortex core region whilst minimising "lost" particles from the sheet, due to the through plane component. Processing was carried out using LaVision DaVis 6.2 software with a multi-pass, cross-correlation algorithm with interrogation window shifting and deformation. The area imaged by the camera was 40.5mm x 30.6mm and the final window size was 32 pixels with 50% overlap giving velocity vectors on a grid of 0.47mm. Seeding was achieved using a Dantec 2010 smoke generator using "Safex Super" smoke fluid at the tunnel inlet. Four measurement planes were used at 765mm, 1115mm, 1465mm and 1815mm from the test section entrance and the model position could also be altered to provide intervening measurement positions. Two wire mesh grids were used to increase the free stream turbulence intensity and had a mesh size of 12.7mm and 7.0mm and wire size 1.25mm and 0.75mm respectively. The grids always placed at a position 57.0mm and 97.0mm upstream of the 150mm and 70mm chord model respectively ensuring that the turbulence intensity for each model remained the same for a given grid regardless of model position.

Measurements of the free-stream turbulence intensity in the clean tunnel and with the grids were performed using a Dantec Streamline hot-wire system. This comprised a Dantec model 55P11 single miniature hot wire, with 5 micron diameter platinum plated tungsten wire 1.25mm in length. The wire was calibrated in a jet and a fourth order polynomial fitted to 15 calibration points and used to convert voltage to velocity. Each measurement comprised 60 ksamples at 2kHz.

3.0 Data reduction method

In this section the method used to extract data corrected for the effects of wandering is described, hereafter referred to as the "PIV method" to distinguish it from the theory of Devenport et al (1996) to which it is compared in section 4.0. During data acquisition, 1050 double-frame images of the flow were recorded at each stream-wise position at a rate of approximately 5Hz and in batches of 150 in short succession, giving a statistically large sample within the constraints of data storage capacity and processing time. Each double-frame image records the instantaneous flow field and therefore position of the vortex at that instant in time. As the data rate is low, compared to the expected frequencies of motion of the vortex, the individual frames do not describe a time series history of the exact motion of the vortex, but merely give discrete samples of it. Thus, the principle of the method demonstrated in this paper is as follows:

1. An algorithm is used to locate the instantaneous centre position of the vortex in each individual PIV vector field. This gives the current displacement vector of the vortex (i.e. instantaneous position minus mean position over the data set).
2. Each individual data field is then moved by its displacement vector such that it is "re-centred" to a common vortex centre position.

3. Normal procedure is then used for calculating mean velocities and Reynolds stresses for the re-centred data and extracting other flow characteristics of interest for example, vortex core radius, peak tangential velocity and vortex strength.

It should be noted that in contrast to the theory of Devenport et al (1996) this method makes no assumption about the nature of wandering as it directly determines the vortex centre positions. In the study of vortex merger by Cerreteli and Williamson (2003) the authors determine the centre position of the vortex from the vorticity field as the peak (positive or negative) vorticity location. Such a method introduces an error in the centre position because the vorticity value will naturally lie at discrete grid node locations. Therefore, in this study, in order to improve accuracy, the peak vorticity location is used as the first approximation to the centre position and this is then improves by finding the minimum in the cross stream velocity field, that is the position where V=W=0. This is performed by the method illustrated in figure 1: First the grid nodes over an area surrounding the point with peak vorticity are located. The size of this area is set before hand and in the current study was 6 x 6 nodes corresponding to an area encompassing approximately half the vortex core diameter. The method then uses two "cross hairs" which traverse across the interrogation region in steps of $\Delta/100$ where Δ is the grid spacing. At each step the velocity component normal to the cross hair is summed up along the cross hair, using bi-linear interpolation of the velocity field. The vortex centre position in each direction then corresponds to the minimum of the sum, and as can be seen in the example shown in figure 1 this deviates from the position of maximum vorticity. Once the vortex centre is determined other parameters of interest can be derived including the radial distribution of circulation, core radius and peak tangential velocity. The peak tangential velocity is found by azimuthally averaging the tangential velocity component around circular paths of increasing radius. In this study radius was incremented in 0.1mm steps. Similarly, the core radius was the position at which the peak tangential velocity was found. The vortex strength was defined as the circulation at twice the core radius, this encompassing 99% of the circulation for an ideal Lamb-Oseen vortex profile. This definition does not encompass all of the circulation in the wake flow, which also includes that contained within the trailing edge shear layer, which gradually rolls-up around the vortex core, and is unknown due to the limited field of view relative to the overall size of the wake, but provides a basis for comparison. All of the above procedure was implemented in a purpose-written C++ program.

The centre finding algorithm was tested in a Monte-Carlo simulation using artificially generated vector fields with Lamb-Oseen vortices. The primary variable affecting the accuracy is the ratio of the vector grid spacing to the physical size of the flow feature of interest which may be characterised by the vortex core size. Thus, ten data sets were created with vector grids ranging from Δ=0.05 to 0.5 times the vortex core radius. The velocity field was chosen to be approximately representative of those measured in the wind tunnel with a core radius of r_c= 4.0mm and peak tangential velocity of 8.0m/s. Each data set consisted of 100 vector fields, with vortex centre positions varied at random according to a bi-variate Gaussian pdf with standard deviation wandering amplitudes set to $\sigma_y=\sigma_z=r_c/2$ and correlation coefficient of e=0.25. The results are presented in figure 2 showing the rms error in the y and z positions of the vortex as determined by the centre

finding algorithm from the original known positions of the vortex. This shows that even with a coarse grid spacing of $\Delta/r_c=0.5$ the rms error in centre position is very small at $0.005r_c$. The effect of this error and the subsequent bi-linear interpolation of the individual velocity fields, on information derived from the results can be seen in figures 3 and 4. Figure 3 shows the mean tangential velocity profile of the re-centred data for varying grid spacing in comparison with the original Lamb-Oseen velocity profile used to create the data sets. As can be seen, with the smallest grid spacing of $\Delta/r_c=0.05$, the profile is recaptured well with the peak tangential velocity slightly under-predicted by 1.4%. With increasing grid spacing the bi-linear interpolation scheme gives increasingly poor results as can be clearly seen at $\Delta/r_c=0.5$. Similarly, figure 4, which shows the cross-stream fluctuation energy, k, shows increasing peaks with grid spacing, at locations of maximum change in the velocity gradients where the bi-linear scheme introduces errors. In the present experiment the ratio of grid spacing to core radius is of the order of 0.1 which it may be expected will introduce errors in the peak tangential velocity of approximately 2%. Higher-order interpolation of the velocity field during re-centring may reduce these errors, but this has not been attempted in this study.

4.0 The effect of vortex strength on wandering

In this section results are presented from four data sets taken with the 70mm chord wing at a stream-wise position of x/c=22.9 and at angles of attack of 4, 6, 8, and 10 degrees. These results are used to demonstrate the effect of wandering on data derived from measurements and the relationship between wandering amplitude and vortex strength. The wandering correction theory of Devenport et al (1996) is tested and compared with the same results from the PIV method.

Mean radial profiles of tangential velocity are shown in figure 5, extracted from the non-re-centred data and the re-centred data. The wandering correction theory of Devenport was implemented in the high-level programming language MathCAD and has independently been used to correct the non re-centred profile for the $\alpha=6°$ and 8° cases. As expected, the effect of wandering, in each case, is to produce an enlarged vortex core with lower peak tangential velocity. Values of core radius and peak tangential velocity are given in table 1 and the wandering amplitudes and correlation coefficients resulting from the PIV and Devenport correction methods are shown in table 2. Comparison of the core parameters listed in table 1 shows that failure to account for wandering results in up to a 12.5% over prediction of the core radius and 6% under prediction of the peak tangential velocity. These errors are greatest for the $\alpha=4°$ case which displayed the greatest wandering amplitude. The good agreement between the PIV corrected data and the prediction of the Devenport theory in both the core parameters shown in table 1 and the wandering amplitudes shown in table 2 should be noted. Figure 6 shows a probability density plot of vortex position for the $\alpha=8°$ case which shows this to be uni-modal and approximately Gaussian in form. Therefore the implicit assumption of Devenport, that the wandering motion of the vortex can be described by a bi-variate Gaussian pdf appears to be valid, thus the good agreement between the corrected data from the PIV method and the Devenport method may perhaps be expected. Inspection of figure 5 shows that there is a disparity between the velocity profile outside of the vortex core predicted by the

Devenport method and that from the PIV method in the α=8° case, but not the α=6° case indicating some error in the Devenport correction scheme in this case.

Fluctuations in the flow characterised by the Reynolds stress components, $\overline{v^2}$, $\overline{w^2}$ and $\overline{vw^2}$ are shown in figure 7. The left-hand side of figure 7 shows the fluctuations computed from the uncorrected data and these have the expected pattern, also reported by Devenport et al (1996) and Chow et al (1997). The right-hand side of the same figure shows the fluctuations calculated from the re-centred data using the PIV method and, on the same contour scale, all of the apparent fluctuations have disappeared. Residual values (which are indistinguishable from the background) are of the same order as those found in section 3 and are due to errors arising from bilinear interpolation of the data. This finding therefore supports the conclusion that, at least at these stream-wise distances behind the wing the vortex core is laminar and the apparent unsteadiness in the uncorrected data is entirely due to wandering.

The linear reduction in wandering magnitude with vortex strength is shown in figure 8. This suggests that the mechanism responsible for wandering is not self induced as proposed by Rokhsaz (2000) in which case it would be expected that wandering would increase with vortex strength. This result further suggests that the vortex is responding to an external influence, for example free-stream turbulence, and that it becomes less susceptible as the vortex strength is increased whilst the strength of the latter remains the same. In all cases the motion of the vortex is weakly negatively correlated, but by an amount which does not appear to vary monotonically with vortex strength.

5.0 Vortex development with stream-wise distance

In this section results are presented for both wing models as a function of stream-wise distance in the clean tunnel. Free stream turbulence levels are varied for the 70mm chord wing using two turbulence grids placed upstream of the model.

Measurements of turbulence intensity made on the tunnel centreline with no wing model present and at stream-wise distances from x/c=-1.0 to x/c=20.5 are shown in figure 9 (throughout this section stream-wise distance is normalised by c=70mm, including data plotted for the 150mm wing). In the clean tunnel, with no turbulence generating grid, turbulence intensity remains at ~1% throughout the test section. Both grids generate increases, that from the 7.0mm grid decaying faster than the 12.7mm grid and both reaching the same level of 1.2% at the furthest stream-wise position. Given that the models were moved throughout the test section with the measurement plane fixed at one of four positions it was also verified that consistent turbulence levels were produced behind the grids independent of there actual stream-wise position and this was found to be the case within 5%. The variation in rms wandering magnitude with stream-wise position for each of the four flow configurations is shown in figure 10 and in each case a linear growth is observed. The initial value responds directly to the varying turbulence intensity levels with that with the 12.7mm grid 55% greater than the clean tunnel and the 7.0mm grid intermediate. The rate of growth is lower with either turbulence grid to that in the clean tunnel, suggesting that the upstream turbulence intensity does not effect the

final wandering amplitude and that, whilst wandering increases with stream-wise distance, it is also a function of the local turbulence intensity. Small decreases in the strength of the vortices were observed with the turbulence grids present (<5%), however if this were a large factor in the wandering amplitudes presented, then it would be expected that the growth rate would be higher in these cases than in the clean tunnel, which is not the case. Comparison of the 70mm and 150mm chord wings in the clean tunnel demonstrates the variation in the rate of growth in wandering with a larger change in vortex strength. Here a 100% increase in vortex strength produces a 33% decrease in growth rate. The correlation coefficient, shown in figure 11, demonstrates that for all the flow configurations, apart from one outlier, the wandering motion is weakly negatively correlated and in general the correlation increases with stream-wise distance, although, as was observed in figure 8, the variation for the individual flow configurations can not be said to be monotonic and further conclusions from this data are not possible.

Corrected profiles of tangential velocity are shown for the 70mm chord wing in the clean tunnel at various stream-wise positions in figure 12. Over this range, x/c=1 to x/c=23, core radius increases by 41% and peak tangential velocity decreases by 20%. This can be compared with 47% and 25% respectively if the data were not corrected for wandering. The variation of core radius and peak tangential velocity with stream-wise distance are plotted for each of the three 70mm chord flow configurations in figure 13a and b. Both quantities show a linear variation at approximately the same rate for each of the flow configurations. The peak tangential velocity is consistently higher in the clean tunnel than with either turbulence grid indicating that, as might be expected, the presence of the grid upstream of the wing effects the formation of the vortex and variation of the turbulence intensity, as attempted here, is not a independent test. The variation of core radius and peak tangential velocity as a function of time for a Lamb-Oseen vortex through viscous diffusion are given by:

$$r_c = \alpha\sqrt{\nu\left(t + t_0\right)} \qquad [1]$$

$$V_\theta = \frac{\beta \cdot \Gamma}{\sqrt{\nu\left(t + t_0\right)}} \qquad [2]$$

where α and β are constants equal to 2.241 and 0.051 respectively (Hubbard (2004)). These variations are also shown in figure 13a and b, where t_0 and Γ have been selected to match the experimental values of core radius and peak tangential velocity at x/c=1 in the clean tunnel. The experimental data for each flow configuration displays a more rapid growth in core radius than the theoretical case, yet a slower decrease in peak tangential velocity. Similarly Devenport et al (1996) also observed a greater rate of growth in core radius, although they attributed this to uncertainty in their wandering correction method, whereas our data suggests this is a real flow phenomena. The slower rate of decrease of the peak tangential velocity than the theoretical case may be due to the extra complications present in the experiment, that is the gradual roll-up of the shear layer from the trailing edge (which is likely to contain 50% of the circulation in the wake at the first stream-wise position (Heyes et al (2003)); i.e. Γ does not remain constant with time.

6.0 Discussion and conclusions

This paper presents a method for correcting for the effects of unsteadiness in vortex wake flows due to the phenomenon of vortex wandering. This permits the "true" mean velocity field of the vortex to be determined. This is possible by interrogation of instantaneous PIV vector fields and locating the position of the vortex numerically using a purpose written algorithm. Knowledge of the instantaneous vortex position then allows re-alignment of the velocity fields such that the centre positions are coincident. The method has been tested using a Monte-Carlo simulation of PIV vector fields and the accuracy of the corrected data was found to be dependent on the vector grid spacing, and limited by the bi-linear interpolation method used when re-centring the data. For data representative of that of the experiment the actual velocity profile of the vortex could be re-captured with a 1.4% error in the peak tangential velocity.

Data was presented showing a linear decrease in wandering amplitude with increasing vortex strength and it was demonstrated that fluctuations in the mean flow field, characterised by the Reynolds stresses, were entirely due to wandering and that the vortices in these cases were laminar in agreement with the findings of Devenport et al (1996). Correction of the data by the method proposed by Devenport et al (1996) showed good agreement of core radius and peak tangential velocity with those obtained with the PIV method used herein. Probability density functions of vortex position showed this to be uni-modal and of approximately Gaussian form an assumption which was implicit in the Devenport method, although not confirmed by those authors.

Measurements of wandering amplitude with stream-wise position in varying background turbulence levels show that the former increases linearly with stream-wise distance with growth rate decreasing with increasing initial turbulence levels. This finding suggests that whilst wandering increases with stream-wise distance it also responds to the local background turbulence levels. The present data does not permit any conclusion to be drawn as to whether it is free stream turbulence which perturbs the vortex core or whether it is turbulence in the shear layer rolling up around the core which is responsible. The horizontal and vertical components of the wandering motion were found to be weekly negatively correlated and increasingly so with stream-wise distance and vortex strength, but the variation was not monotonic for any individual flow configurations and no further conclusion have been drawn.

Corrected velocity profiles for one configuration showed a 41% increase in core radius and a 20% decrease in peak tangential velocity over a stream-wise range of 21.9c. These variations were shown to be approximately linear and the increase in core radius was greater than that predicted for a Lamb-Oseen vortex undergoing viscous diffusion whilst the decrease in peak tangential velocity was less, probably due to the roll up of the surrounding wake.

The method presented herein has been demonstrated to be a effective for extracting reliable data from vortex wake measurements and should be widely applicable to more complicated flow configurations including turbulent vortices.

Acknowledgements

The authors would like to acknowledge the financial support of EPSRC.

References

Baker GR, Barker SJ, Bofah KK, Saffman PG, (1974) Laser anemometer measurements of trailing vortices in water, Journal of Fluid Mechanics, (65) 325-336.

de Bruin AC, Hegen SH, Rohne PB, Spalart PR, (1996) Flow field survey in trailing vortex system behind a civil aircraft model at high lift, AGARD CP 584: The Characterisation & Modification of Wakes from Lifting Vehicles in Fluid.

Cerreteli C, Williamson CHK, (2003), The physical mechanism for vortex merging, Journal of Fluid Mechanics, (475) 41-77.

Chow JS, Zilliac GG, Bradshaw P, (1997), Mean and Turbulence Measurements in the Near Field of a Wingtip Vortex, AIAA Journal (35) 1561-1567.

Cliffone DL, (1976), Vortex interactions in Multiple Vortex Wakes behind Aircraft", Journal of Aircraft, (14:5) 440-446.

Devenport WJ, Rife MC, Liapis SI, Follin GJ, (1996), The structure and development of a wing-tip vortex, Journal of Fluid Mechanics, (312) 67-106.

Gursul I, Xie W, (2000), Origin of Vortex Wandering over Delta Wings, Journal of Aircraft, (37:2) 348-350.

Heunecke K, (2002), From Formation to Decay Extended-time Wake Vortex Characteristics of Transport-type Aircraft, AIAA conference proceedings 2002-3265.

Heyes AL, Hubbard SJ, Marquis AJ, Smith DA, (2003) On the Roll-up of a Vortex Sheet in the Very Near Field, Proceedings of the IMechE Part G: Journal of Aerospace Engineering, (217:5) 262-268.

Hubbard SJ, (2004), Computation of wake vortex related flows using discrete vortex and quasi three-dimensional Navier-Stokes methods, PhD Thesis, University of London.

Jacquin L, Fabre D, Geffroy P, Coustols E, (2001), The properties of a transport aircraft wake in the extended near field: An experimental study, AIAA conference proceedings 2001-1038.

Rokhsaz K, Foster SR, Scott Miller L, (2000), Exploratory Study of Aircraft Wake Vortex Filaments in a Water Tunnel, Journal of Aircraft, (37:6) 1022-1027.

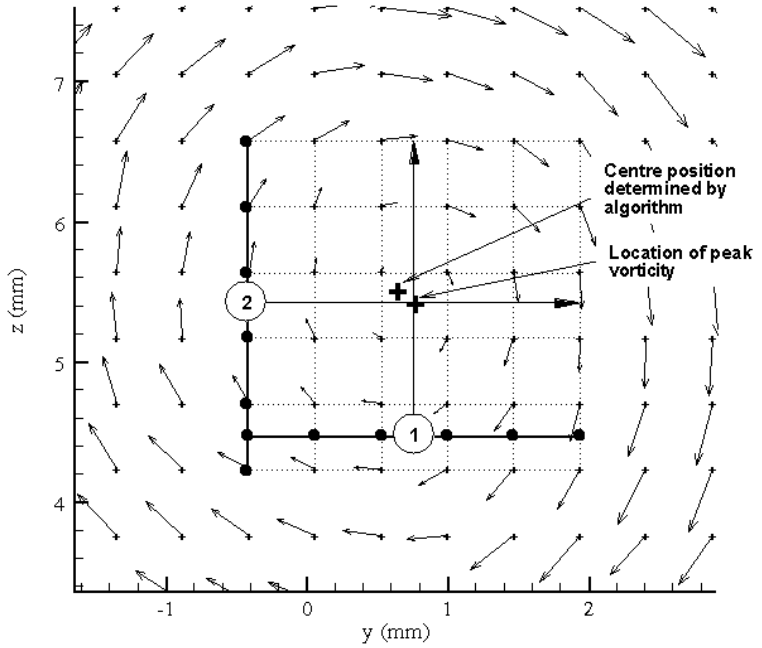

Figure 1. Diagram illustrating vortex centre finding algorithm.

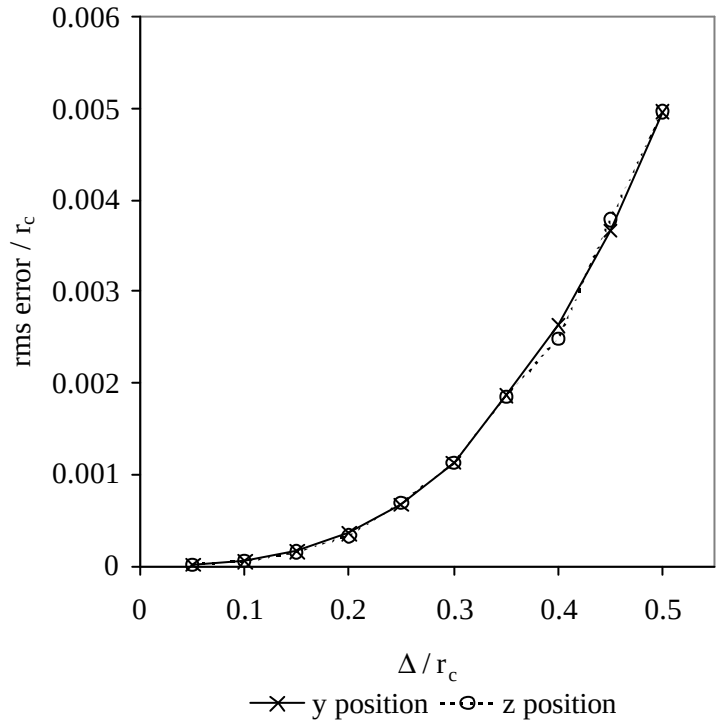

Figure 2: rms error in centre position with varying grid spacing.

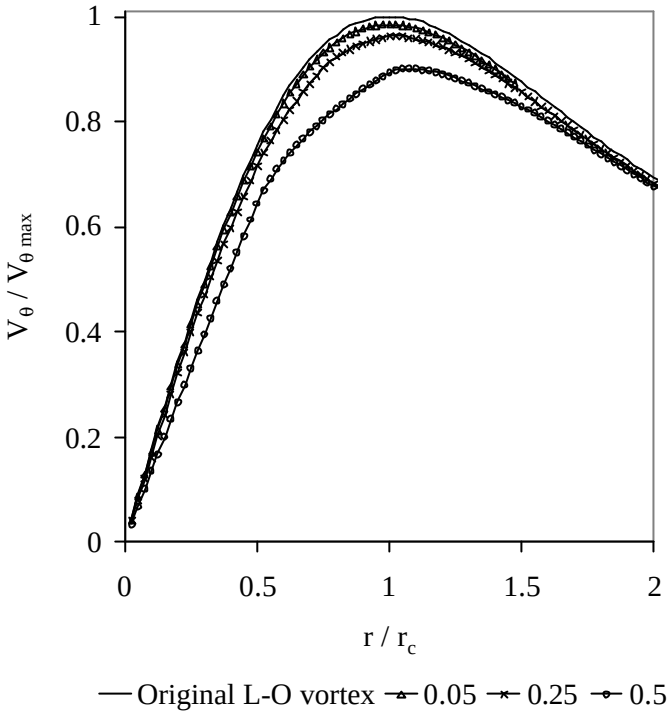

Figure 3. Mean tangential velocity profile extracted from re-centred data with varying grid spacing, Δ/r_c.

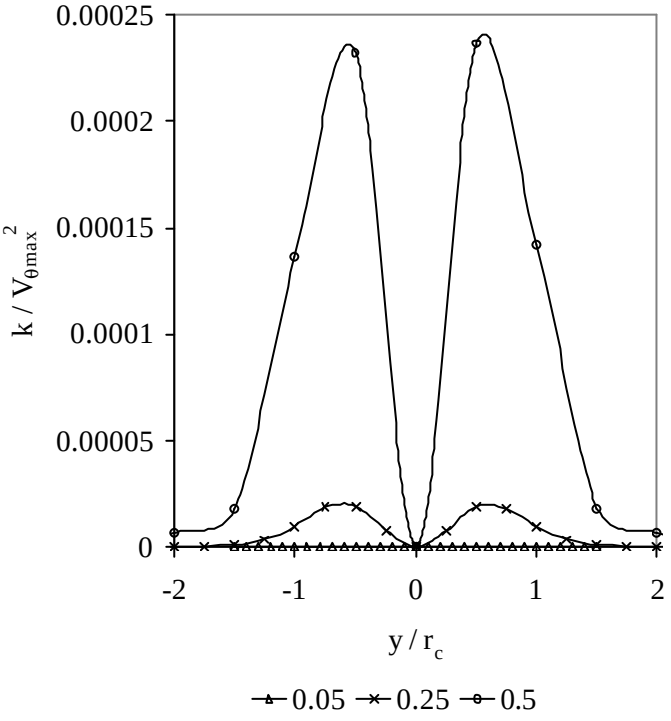

Figure 4. Cross-stream fluctuation energy after re-centring with varying grid spacing, Δ/r_c.

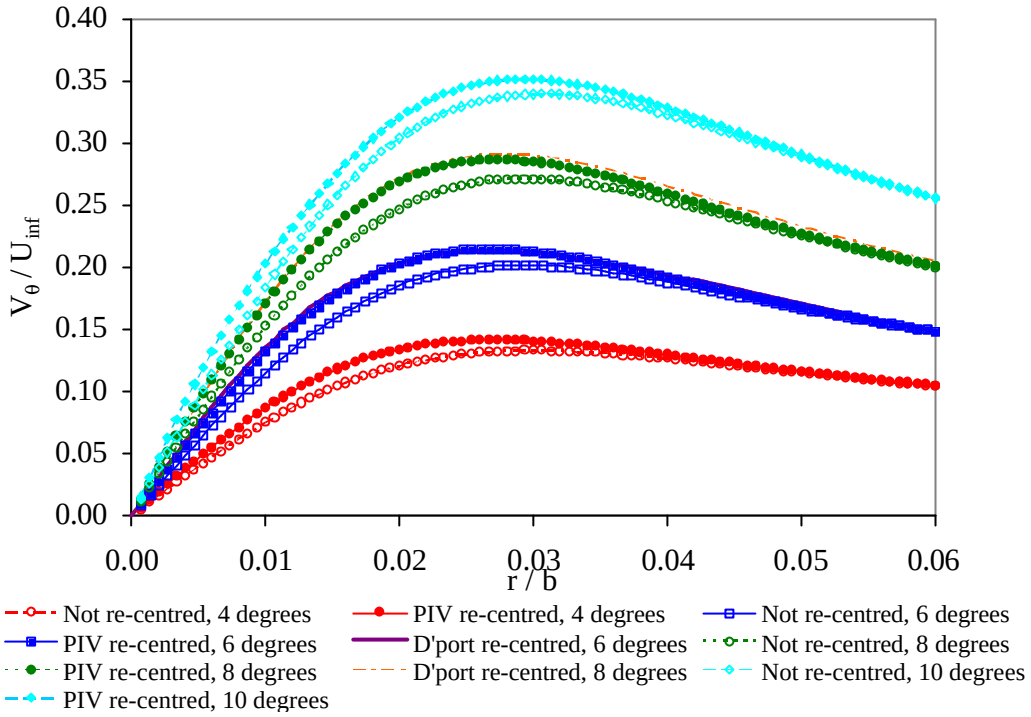

Figure 5. Radial profiles of tangential velocity for non re-centred and re-centred data using the PIV method and the Devenport method.

α (degrees)	Core radius r_c (mm)			Peak tangential velocity $V_{\theta_{max}}$ (m/s)		
	Non re-centred	PIV re-centred	Devenport re-centred	Non re-centred	PIV re-centred	Devenport re-centred
4	4.5	4.0	-	2.87	3.05	-
6	4.4	4.0	4.0	4.36	4.64	4.60
8	4.4	4.1	4.2	5.86	6.19	6.29
10	4.6	4.4	-	7.33	7.59	-

Table 1. Vortex core parameters for non re-centred and re-centred data.

α (degrees)	PIV Method			Devenport method		
	σ_v (mm)	σ_z (mm)	e	σ_v (mm)	σ_z (mm)	e
4	0.97	1.17	-0.29	-	-	-
6	0.97	1.00	-0.37	0.97	1.00	-0.37
8	1.05	0.83	-0.18	1.05	0.83	-0.19
10	0.93	0.85	-0.11	-	-	-

Table 2. Wandering amplitude data for PIV method and Devenport method.

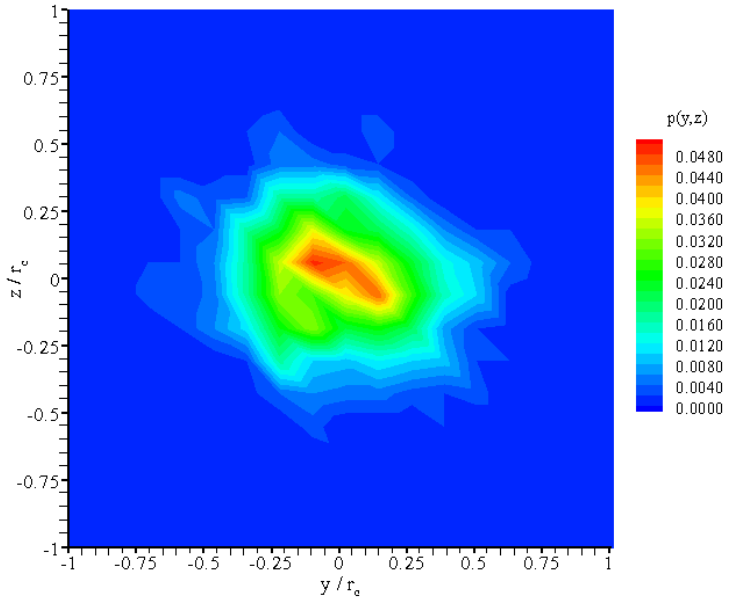

Figure 6. Probability density plot of vortex position for α=8° case at x/c=22.9.

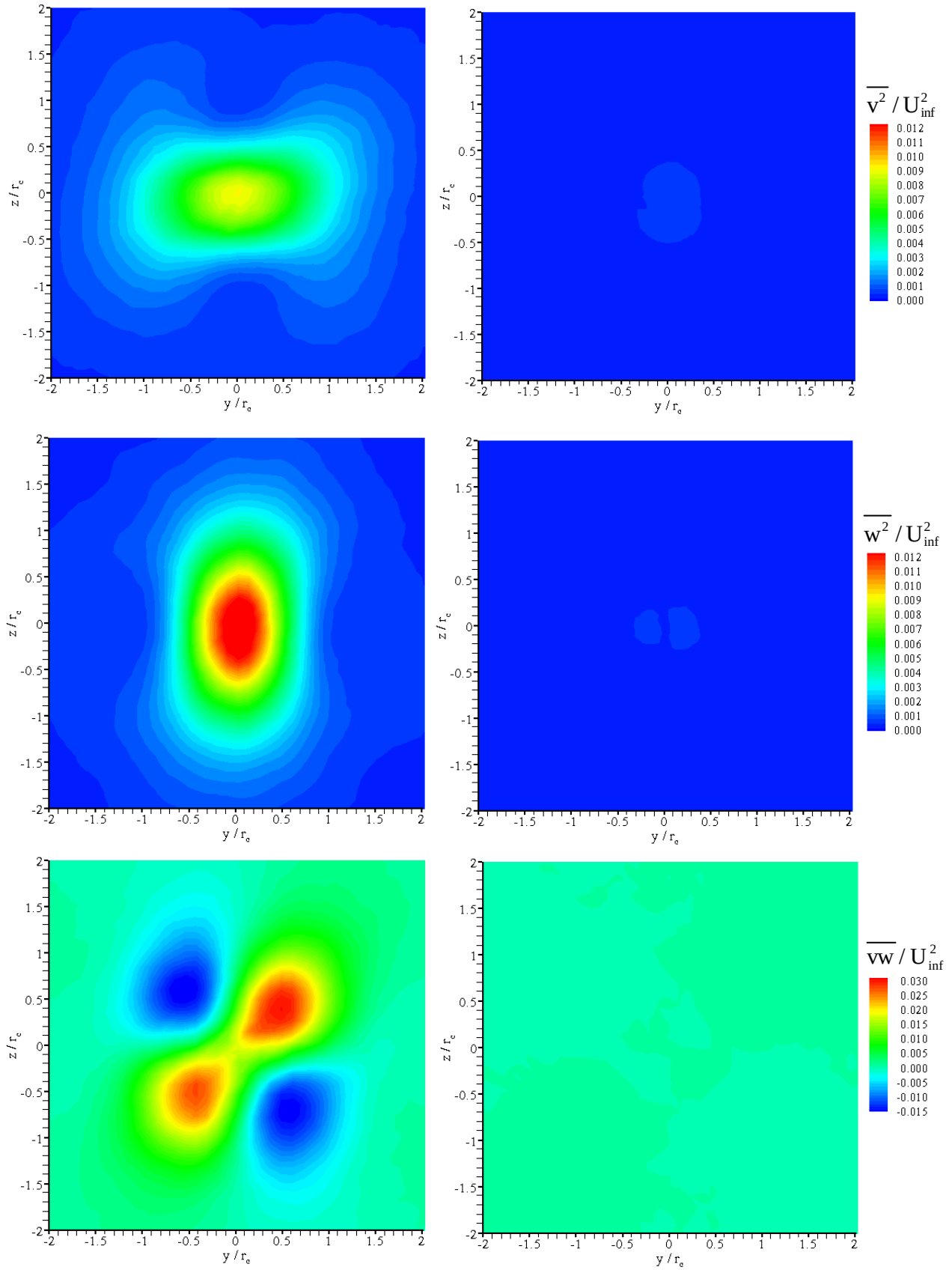

Figure 7. Reynolds stress components calculated from non re-centred data (left hand side) and re-centred data (right hand side).

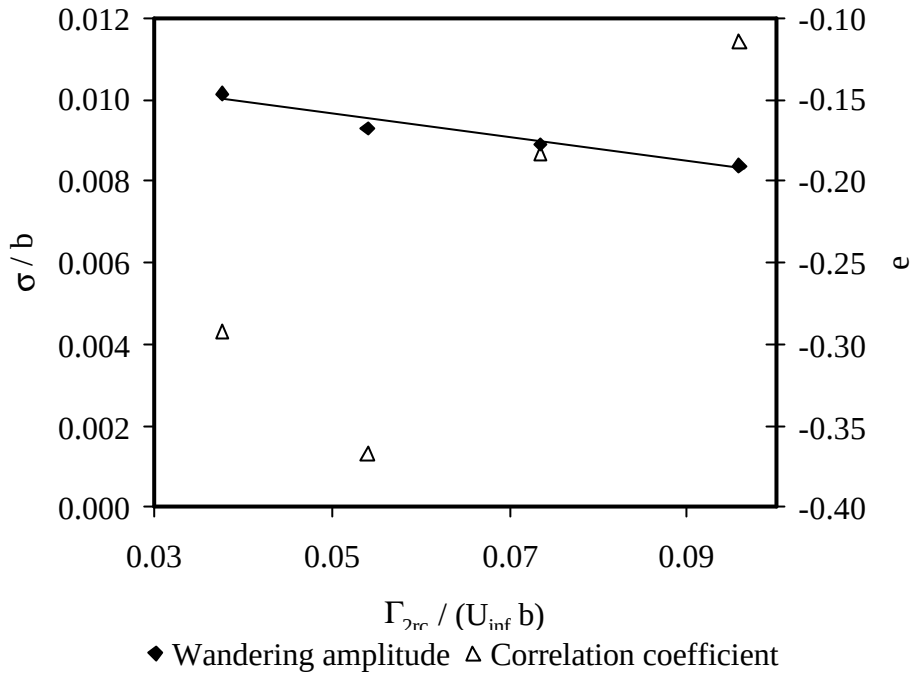

Figure 8. Variation of wandering amplitude and correlation coefficient with vortex strength.

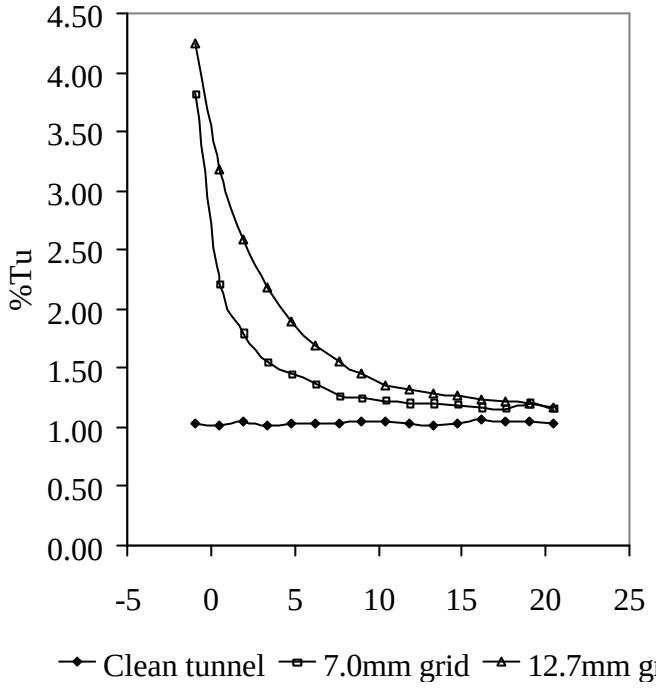

Figure 9. Variation of turbulence intensity with stream-wise distance.

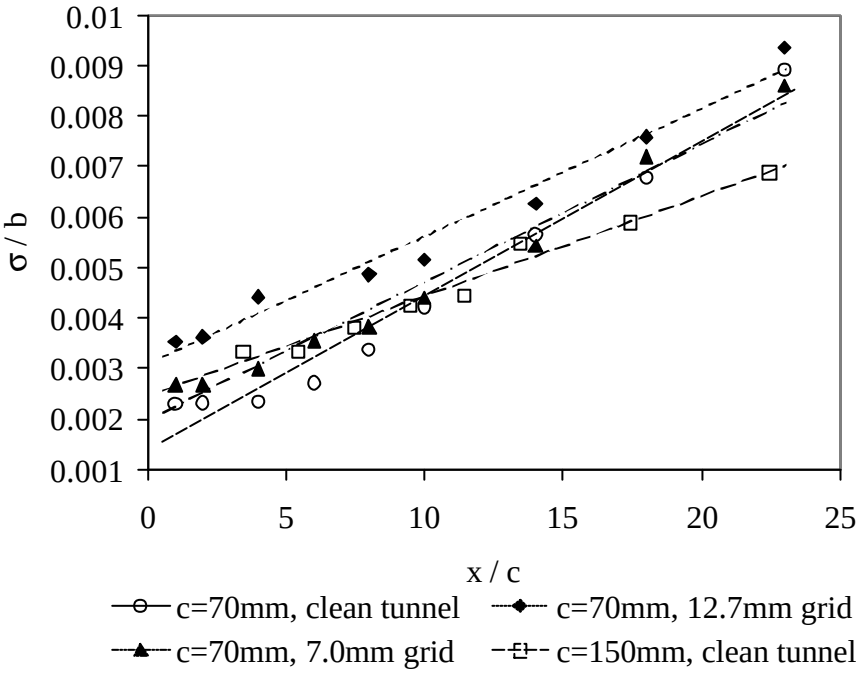

Figure 10. Variation of wandering amplitude with stream-wise distance.

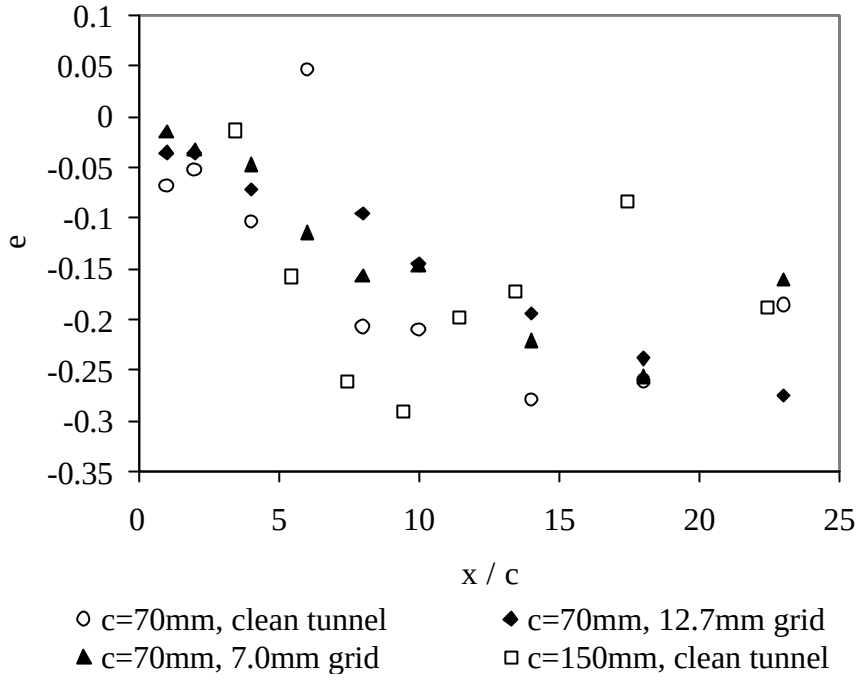

Figure 11. Variation of correlation coefficient with stream-wise distance.

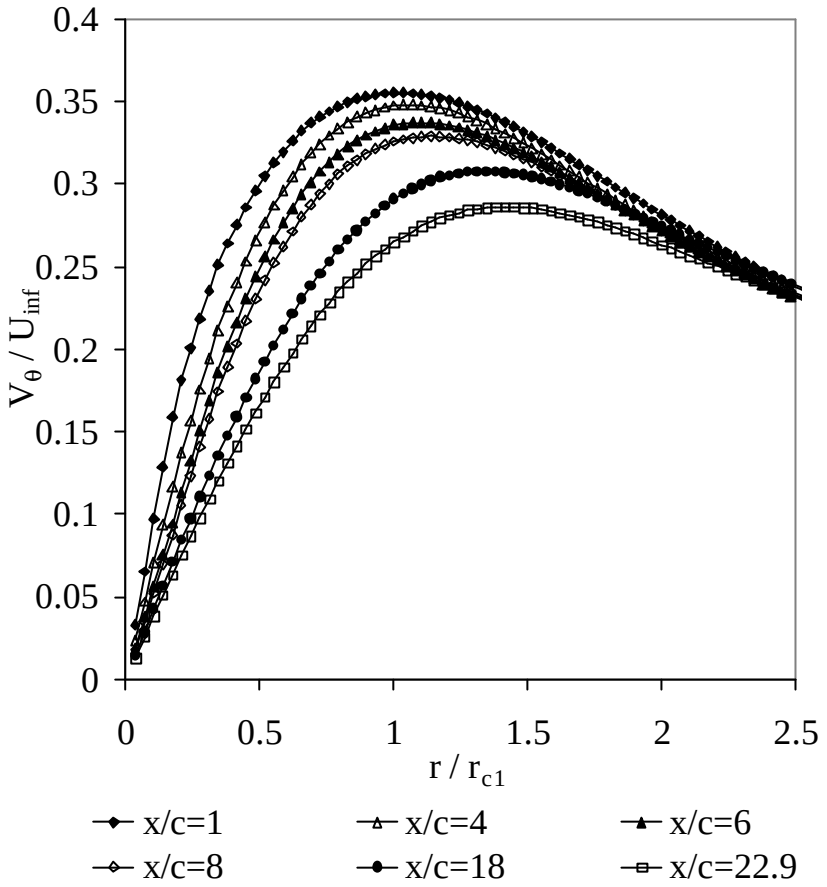

Figure 12. Radial profiles of tangential velocity for 70mm chord wing with stream-wise distance in the clean tunnel.

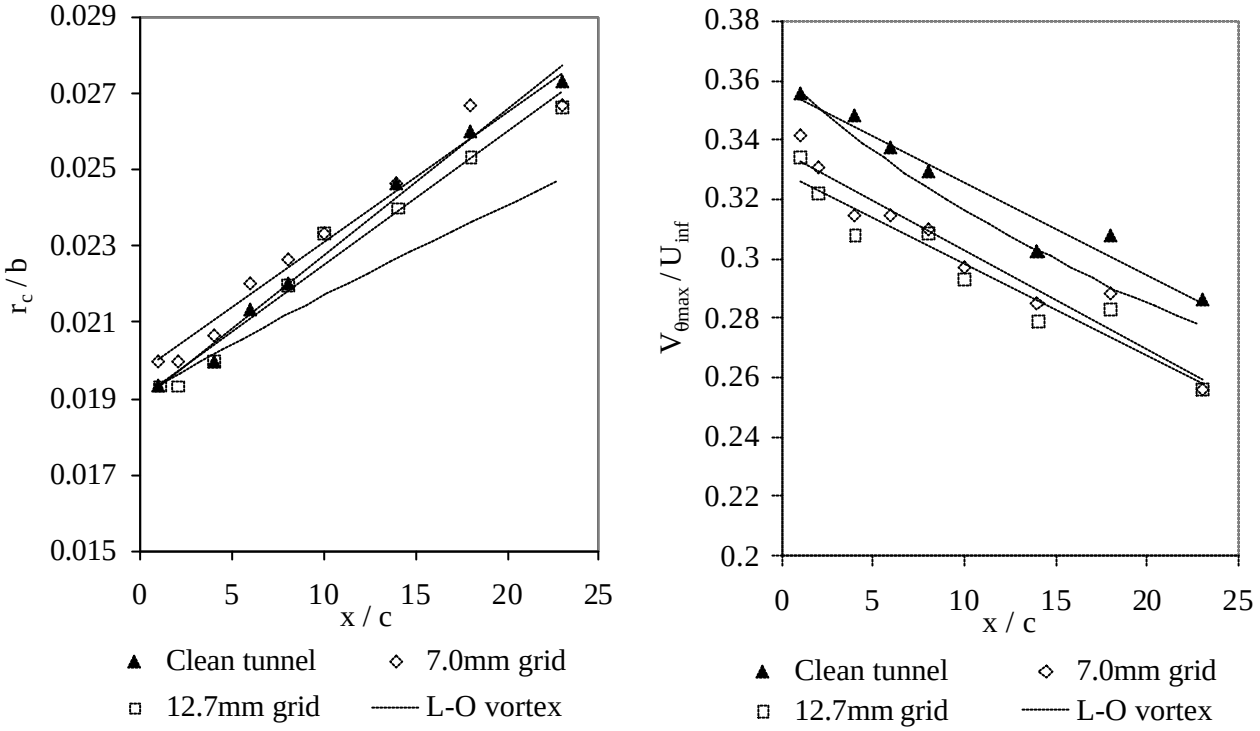

Figure 13. (a) Variation of core radius with stream-wise distance. (b) Variation of peak tangential velocity with stream-wise distance.